

# Formation of the ferromagnetically bound spin pairs in the bond-diluted spin-gap antiferromagnet PHCC.

V.N. Glazkov,<sup>1,2,\*</sup> G. Skoblin,<sup>1,2</sup> D.Hüvonen,<sup>3,†</sup> T.S. Yankova,<sup>3,‡</sup> and A.Zheludev<sup>3</sup>

<sup>1</sup>*Kapitza Institute for Physical Problems RAS, Kosygin str. 2, 119334 Moscow, Russia*

<sup>2</sup>*Moscow Institute of Physics and Technology, 141700 Dolgoprudny, Russia*

<sup>3</sup>*Neutron Scattering and Magnetism, Laboratory for Solid State Physics, ETH Zürich, 8006 Zürich, Switzerland*

(Dated: March 18, 2019)

We report results of the electron spin resonance study of a spin-gap antiferromagnet  $(\text{C}_4\text{H}_{12}\text{N}_2)(\text{Cu}_2\text{Cl}_6)$  (nicknamed PHCC) doped with Br. For all doping levels, absorption intensities at the temperatures above 3...4 K follows model of a spin-gap magnet. We have found that up to 10% doping contribution of the random defects to the absorption spectra remains about 0.1% per copper ion, almost the same as in the pure system. Increase of the bromine concentration leads to the systematic broadening of the ESR absorption line indicating reduction of the quasi-particles lifetime. At the temperatures below 3K highly-doped (nominal Br content  $x \geq 5\%$ ) samples demonstrate behaviour qualitatively different from that of the pure and low-doped samples. The low-temperature electron spin resonance absorption spectra of the highly-doped samples are analogous to that of the gapless  $S = 1$  object. We suggest that bromine doping results in the formation of a certain number of the ferromagnetically bound Cu-Cu pairs submerged in the spin-gap matrix.

PACS numbers: 75.10.Kt, 76.30.-v

Keywords: low-dimensional magnet

## I. INTRODUCTION.

Spin-gap antiferromagnets have been actively studied during the last decades. Because of particular geometry of the spin-spin interactions (frequently featuring dimer motives) these systems of strongly exchange coupled spins do not order antiferromagnetically, but remain in disordered spin-singlet ( $S = 0$ ) state down to the lowest temperatures. Stability of the singlet state is ensured by the energy gap of exchange origin  $\Delta$  separating the ground state from the magnetic triplet ( $S = 1$ ) excitations. Among the examples of such systems are: spin-Peierls magnet  $\text{CuGeO}_3$ ,<sup>1</sup> dimer magnet  $\text{TiCuCl}_3$ ,<sup>2</sup> various Haldane magnets (e.g.,  $\text{PbNi}_2\text{V}_2\text{O}_7$ ,<sup>3,4</sup> or organo-metallic compound  $\text{NENP}$ )<sup>5</sup> and various spin-ladder systems.<sup>6</sup>

Application of external magnetic field leads to the Zeeman splitting of the triplet states and to the lowering of the energy of one of its substates. This leads to a quantum critical point at a certain critical field  $H_c \simeq \Delta/(g\mu_B)$ . If spin subsystem is three-dimensional, then a field induced antiferromagnetically ordered phase is formed above the critical field.<sup>7</sup>

Controlled introduction of defects is another way to affect stability of the ground state. In the case of magnetic systems bond-doping, i.e. introduction of the defects that affect interspin couplings but do not affect magnetic sublattices, is of particular interest as a way to realize different random coupling models. Theoretical models considering such a systems make different interesting predictions including formation of a glass-like state<sup>8</sup> or a random singlet state.<sup>9,10</sup> This mechanism was already exploited in the study of random-bond systems  $\text{IPA-CuCl}_3$ ,<sup>11,12</sup>  $\text{Sul-Cu}_2\text{Cl}_4$ ,<sup>13</sup> and  $\text{DTN}$ .<sup>14</sup>

Recently found organo-metallic compound

$(\text{C}_4\text{H}_{12}\text{N}_2)(\text{Cu}_2\text{Cl}_6)$  (abbreviated as PHCC for piperazinium hexachlorodocuprate) is a good test model to study both effects of impurities and quantum criticality. The pure compound is well characterized by a variety of techniques including bulk measurements, elastic and inelastic neutron scattering<sup>15-17</sup> and electron spin resonance.<sup>18</sup> These measurements have confirmed existence of the energy gap  $\Delta = 1.02$  meV, triplet nature of magnetic excitations and closing of the energy gap by the magnetic field above approximately 8T. Inelastic neutron scattering experiments revealed presence of at least six relevant exchange couplings,<sup>15</sup> the exchange couplings geometry can be envisioned as a 2D set of moderately coupled spin-ladders with the dominant interaction on the rung of the ladder and some frustrating couplings.

This system allows to perform a substitution of chlorine ions mediating the interspin interactions by bromine with the Br concentration above 10%. As it was shown by neutronographic and calorimetric experiments<sup>19-21</sup> doping results in the increase of the gap and critical field, in the broadening of the excitations spectrum and in the change of the critical exponent. The magnons damping in the doped samples turned out to be strongly dependent on the wavevector with damping rate increasing away from the zone center.<sup>20</sup>

In the present paper we present results of the electron spin resonance (ESR) study of the bromine doped PHCC single crystals. High energy resolution of ESR technique and its ability to distinguish between different paramagnetic centers allows us to demonstrate that particular kind of  $S=1$  paramagnetic centers are formed with bond doping. Data suggests that these centers are ferromagnetic Cu dimers at the sites where both superexchange mediating Cl ions are replaced by Br. At the same time,

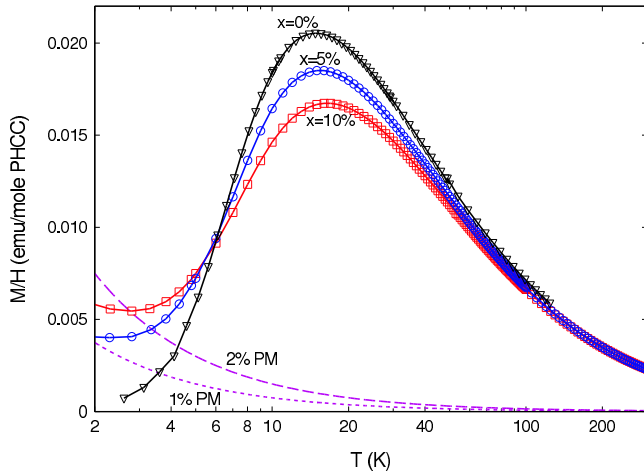


FIG. 1. (color online) Temperature dependency of the magnetization. (Symbols) experimental data for the nominally pure sample and the samples with  $x = 5\%$  and  $x = 10\%$ ,  $\mathbf{H}||c$ ,  $H = 1\text{kOe}$ . (Dashed lines) Curie laws for the  $S = 1/2$   $g = 2.0$  paramagnets with the spin concentrations of 1% and 2% per copper ion.

increase of ESR linewidth indicates reduction of lifetime of the thermally excited triplet excitations.

## II. EXPERIMENTAL DETAILS AND SAMPLES CHARACTERIZATION.

### A. Samples preparation and characterisation.

Samples of pure and bromine diluted not-deuterated PHCC were grown from solution as described in Ref.22. The saturated solution for the growth of pure PHCC was prepared by adding of piperazine  $\text{C}_4\text{H}_{10}\text{N}_2$  (from Sigma Aldrich), dissolved in a minimal amount of concentrated HCl, to  $\text{CuCl}_2 \cdot 2\text{H}_2\text{O}$  (99.99% purity from Sigma Aldrich), dissolved in a minimal amount of concentrated HCl, at a 4:1 molar ratio of  $\text{CuCl}_2$  to  $\text{C}_4\text{H}_{10}\text{N}_2$ . Saturated solution for the diluted crystals was prepared by introducing a proportional amount of  $\text{CuBr}_2 \cdot 2\text{H}_2\text{O}$  and HBr. We will use nominal bromine concentration (determined by the Br to Cl ratio in the initial solution components) for the sample identification. As grown samples have a typical size of  $3 \times 3 \times 5 \text{ mm}^3$  with a well developed plane normal to the  $a^*$ -axis and the longest axis of the sample parallel to the  $c$ -axis.

The quality of the samples was checked by X-ray diffraction on Bruker Apex II diffractometer. It was found that up to the nominal bromine content of 12.5% lattice symmetry remains the same (triclinic) and lattice constants slowly increase.<sup>21</sup> Above 12.5% phase separation was found to occur. Detailed structural analysis<sup>21</sup> have demonstrated that the average bromine concentration is slightly beyond the nominal value and the occupation of different halogen positions is different: bromine

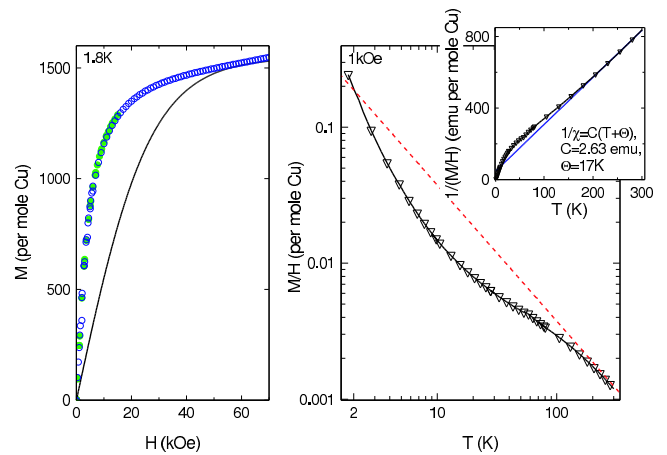


FIG. 2. (color online)  $M(H)$  and  $M(T)$  dependencies for the powder sample with bromine content 100%. Molar magnetization is calculated using tentative chemical formula  $(\text{C}_4\text{H}_{12}\text{N}_2)\text{CuBr}_4$ . (Left panel)  $M(H)$  curve measured at 1.8K. Open symbols correspond to the magnetization measured for the positive field, close symbols are the symmetrically reflected data for the negative fields. Solid curve is a saturation curve calculated for noninteracting spins  $S = 1/2$  with  $g = 2.0$  and concentration 28% per Cu ion. (Right panel)  $M(T)$  curve measured at the field of 1 kOe. Every 5-th point is plotted for clarity. Dashed line on the main panel is a paramagnetic Curie law for the spins  $S = 1/2$  with  $g = 2.0$  and concentration of 100% per copper ion. Solid line at the insert is a Curie-Weiss law with a Curie-Weiss temperature  $\Theta = 17\text{K}$ .

ions enter at almost nominal concentration at the positions responsible for the strongest couplings (rung and leg of the ladder), while bromine occupation of the positions responsible for the interladder couplings is by a factor of three smaller.

The static magnetization of all samples was measured with a Quantum Design MPMS-XL system. The  $M(T)$  curves are shown on Fig.1. All curves demonstrate a broad maximum around 15K and below this temperature magnetization decreases due to the diminishing population of the gapped magnetic excitations. Maximal value of the magnetization at the peak decreases with doping. At low temperatures (below 4K) the exponential decrease changes into a Curie-like increase due to defects, impurities or other paramagnetic objects. The amplitude of the magnetization at low temperatures corresponds to the concentration of paramagnetic defects of about 1% per copper ion for the nominally 5% Br-doped sample and about 1.5% per copper ion for the nominally 10% Br-doped sample.

Additionally, we have attempted to grow a sample with the bromine content of 100% by slow evaporation of the solution. It turned out to be impossible to grow large crystals of the intended material. We were able to obtain only some small flake-like crystals with the dimensions of several millimeters and thickness of the order of 0.1 mm or less. X-ray diffraction shows that these crystals have different lattice: best fits are

obtained for the monoclinic symmetry group  $P2(1)/c$  ( $C_{2h}^5$ ), while PHCC lattice is triclinic, with the lattice constants  $a = 13.2865 \pm 0.0009 \text{ \AA}$ ,  $b = 7.1005 \pm 0.0003 \text{ \AA}$  and  $c = 12.3867 \pm 0.0006 \text{ \AA}$  and the angle  $\beta = (96.655 \pm 0.004)^\circ$ ,  $a$  and  $c$  lattice constants being almost twice as large as those of pure PHCC. Magnetization measurements (Figure 2) showed that the molar high-temperature magnetization calculated with the molar mass of  $(C_4H_{12}N_2)(Cu_2Br_6)$  (hypothetic 100% Br-doped PHCC) is a factor of 1.4 smaller than the expected value for the  $g = 2.0$   $S = 1/2$  paramagnet. Tentatively, the molar mass of a  $(C_4H_{12}N_2)(CuBr_4)$  composition provides a better agreement with the high-temperature susceptibility data. Antiferromagnetic Curie-Weiss temperature found from the high-temperature (200-300 K) data is 17K. Indeed,  $M(T)$  curve (see right panel of Figure 2) bends downwards from the paramagnetic Curie law below 100K indicating the presence of antiferromagnetic interactions. However, at lower temperatures (below 10K) it turns upward and even exceeds paramagnetic Curie curve at the lowest temperature of 2K. This increase can not be ascribed to the paramagnetic defects or impurities as the low temperature  $M(H)$  curve (left panel of Figure 2) almost saturates at about 28% of the saturation magnetization for the noninteracting  $S = 1/2$   $g = 2.0$  spins, but the observed saturation process is faster than for a hypothetical  $S = 1/2$   $g = 2.0$  paramagnet with spin concentration of  $x = 28\%$  approximately by a factor of 3. Note that the estimation of the observed saturation magnetization as about 28% of the nominal value is independent from our ignorance on the exact chemical composition of the bromine compound since it is based on the ratio of the independently measured high-temperature Curie constant and low-temperature magnetization. Combination of the antiferromagnetic Curie-Weiss temperature, reduced saturation magnetization and ferromagnetic-like quick increase of the low-temperature magnetization suggests that the bromine compound probably is an example of a magnet with the competing ferro- and antiferromagnetic interactions.

## B. ESR experiment details

Electron spin resonance experiments were carried out with the help of home made transmission type ESR spectrometers at the frequencies 10-70 GHz and at the temperatures down to 450 mK. For the experiments above 1.5K we used a helium-4 bath cryostat, for the experiments below 1.5K a specially designed multi-frequency ESR spectrometer combined with helium-3 cryostat was used. Highest temperature available in the helium-3 setup was about 6K.

Here we briefly recall some basics of ESR technique that will be necessary to interpret experimental data.<sup>23,24</sup> Resonance absorption appears when the Zeeman splitting of the energy levels becomes equal to the energy of the microwave radiation quantum, for the spin  $S = 1/2$  this

results in the equation  $\hbar\omega_0 = g\mu_B H_{res}$ . If the resonating center has spin  $S > 1/2$  then a so called crystal field splitting of the spin levels can appear, in the simplest case it is described by the axial term in the Hamiltonian  $\hat{H}_{CF} = D\hat{S}_z^2$ . For the case of  $S = 1$  this term splits the spin substates with  $S_z = 0$  and  $S_z = \pm 1$  and resonance conditions (for  $\mathbf{H}||z$ ) become  $g\mu_B H_{res} = \hbar\omega_0 \pm D$ . Direct transition between  $S_z = \pm 1$  sublevels (so called "two-quantum" transition) is forbidden by the selection rules in the axial case, but it can be allowed for the lower symmetry, resulting in the characteristic absorption signal at one half of the usual paramagnetic resonance field  $\hbar\omega_0/2 = g\mu_B H_{2q}$ . Thus, the ESR technique provides the selectivity that allows to distinguish the absorption signals originating from the differing magnetic centers and to identify these centers by their  $g$ -factor and spin.

In our experiment the absorption curves are recorded as a function of the slowly swept magnetic field at the fixed microwave frequency  $\omega_0$ . At the electron paramagnetic resonance conditions the sample absorbs the microwave radiation and the microwave power transmitted through the microwave resonating cavity containing the sample decreases. For a weakly absorbing point sample the decrease of the transmitted microwave power is proportional to the imaginary part of the high-frequency susceptibility  $\chi''(\omega, H)$  for the appropriate polarization of the microwave magnetic field. For a finite size sample the absorption have to be integrated over the sample volume taking into account the variation of the microwave field inside the sample. The proportionality coefficient between the  $\chi''(\omega, H)$  and the decrease of the detector output  $\Delta U/U_0$  is *a priori* unknown, it depends on the microwave fields distribution, cavity Q-factor and other technical details. However, it remains the same for each series of experiments (with the same microwave frequency and the same sample mounting).

If the resonance absorption spectrum consists of a single narrow paramagnetic resonance line (i.e., with the resonance field  $H_{res}$  linear with resonance frequency  $\omega_0$ :  $\omega_0 = \gamma H_{res}$ ), then neglecting the anisotropy of  $g$ -tensor (which also enters a scaling factor) and assuming that the magnetization is far from saturation, Kramers-Kronig relations can be used to scale the integrated intensity of the paramagnetic absorption due to the microwave field perpendicular to the static field with the independently measured static susceptibility  $\chi(0)$ :

$$\begin{aligned} \chi(0) &= \frac{2}{\pi} \int_0^\infty \frac{\chi''(\omega)}{\omega} d\omega \approx \frac{2}{\pi\omega_0} \int_0^\infty \chi''(\omega) d\omega = \\ &= \frac{2}{\pi H_{res}} \int_0^\infty \chi''(H) dH \propto \int_0^\infty \frac{\Delta U}{U_0} dH \quad (1) \end{aligned}$$

This allows to establish the scaling factor for the given experiment and to calculate the imaginary part of the susceptibility in absolute units. This, in turn, allows to estimate the amount of the paramagnetic centers responsible for the different components of the absorption spectrum.

For the isolated paramagnetic center intensity of the ESR absorption due to the transitions between the spin sublevels  $|n\rangle$  and  $|m\rangle$  ( $E_n < E_m$ ) depends on the sub-levels populations and matrix element of the transition.

$$I_{nm} \propto \frac{(e^{-\frac{E_n}{T}} - e^{-\frac{E_m}{T}}) \int_s |\langle n | \hat{\mathbf{S}} \cdot \mathbf{h}_{mw}(\mathbf{r}) | m \rangle|^2 dV}{\sum_k e^{-E_k/T}} \quad (2)$$

here integration is performed over the sample volume to take into account distribution of the microwave field polarizations  $\mathbf{h}_{mw}$  through the sample. Temperature dependency of the selected component intensity is determined by the combination of Boltzman exponents.

The matrix element of the transition determines the selection rules and applicability of the scaling equation Eqn.(1). For the particular case of  $S = 1$  center in the weak crystal field ( $g\mu_B H_{res} \gg D$ ) the magnetic field direction is a quantization axis and the effective anisotropy constant  $\tilde{D}$  is orientation dependent. Then the spin sub-states are classified by the spin projection on the field direction, the main resonance absorption appears on the  $|\pm 1\rangle \leftrightarrow |0\rangle$  transitions, these transitions are excited by the convenient polarization of the microwave magnetic field perpendicular to the static field and the excitation factor  $\int_s |\langle n | \hat{\mathbf{S}} \cdot \mathbf{h}_{mw}(\mathbf{r}) | m \rangle|^2 dV$  is the same for these two transitions. The "two-quantum"  $|1\rangle \leftrightarrow |-1\rangle$  absorption becomes allowed in the higher orders of perturbations and, if the crystal field symmetry is lower than the axial, for the microwave field parallel to the static field. Thus the excitations conditions for the main absorption signals and for the "two-quantum" transition are essentially different.

### III. EXPERIMENTAL RESULTS.

#### A. ESR on the reference sample $x = 0\%$ .

The results of the ESR investigation of the nominally pure ( $x=0\%$ ) PHCC are reported in detail in Ref.18. At high temperatures (above 20K) a single resonance absorption component is observed with an anisotropic  $g$ -factor slightly above 2.0, as it is typical for  $\text{Cu}^{2+}$  ions. The intensity of the ESR absorption follows a temperature dependency of the magnetization with a broad maximum around 20K. Below 20K the ESR absorption loses intensity as the magnetic excitations freeze out. As the population of magnetic excitations drops down, their interaction vanishes and the triplet  $S = 1$  excitations respond to the effective crystal field microscopically originating from different anisotropic spin-spin interactions. This lifts degeneracy of the triplet level and results in the splitting of the ESR absorption line in two main components (Fig.3) corresponding to  $|\pm 1\rangle \leftrightarrow |0\rangle$  transitions and allows the "two-quantum" transition  $|+1\rangle \leftrightarrow |-1\rangle$  at approximately half of the paramagnetic resonance field. We mark these components in the order of increase of resonance field as "A", "B" and "C" for the "two-quantum"

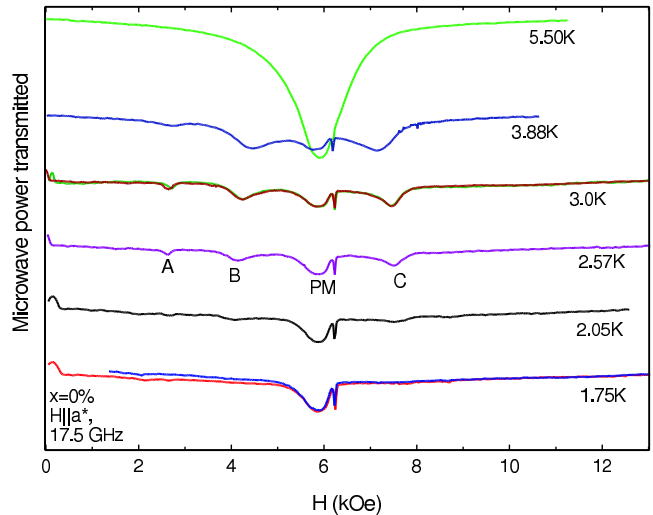


FIG. 3. (color online) Temperature dependencies of the ESR absorption in pure sample at low temperatures. Spectra are offset for better presentation. Spectral components are marked by letters: (A) "two-quantum" transition, (B) and (C) main intra-triplet transitions, (PM) paramagnetic defects and impurities. Narrow absorption line at 6.2kOe is a DPPH marker ( $g = 2.0$ ).

transition and two main components correspondingly. Splitting of the main components and their relative intensities are related to the parameters of the effective crystal field and to the orientation of the anisotropy axes with respect to the field.

Split components continue to lose intensity on cooling and below 2.0K the ESR absorption spectrum mainly consists of the paramagnetic absorption due to the defects and impurities (marked as "PM").

#### B. ESR on the low-doped sample PHXC $x = 1\%$ .

The temperature evolution of the ESR absorption for the low-doped ( $x = 1\%$ ) sample is qualitatively the same as for the pure sample (Fig.4). On cooling below 10K the ESR absorption loses intensity, the ESR line broadens and splits around 4K into three components (again marked as "A", "B" and "C" on Fig.4). These components freeze out on further cooling and at the lowest temperature the ESR absorption spectrum consists of a single line with the  $g$ -factor close to 2.0, which is related to the defects and impurities. Thus, the observed ESR absorption is also mostly due to the triplet excitations

Parameters of the ESR spectra in the pure PHCC and  $x = 1\%$  doped PHXC differs just by the widths of the spectral components. The values of  $g$ -factors (2.064 for the pure compound<sup>18</sup> and  $2.09 \pm 0.03$  for the  $x = 1\%$  PHXC) and the magnitudes of the splitting of the "B" and "C" components ( $3.7 \pm 0.2$  kOe for pure PHCC and  $3.3 \pm 0.3$  kOe, Figs.3, 4) are almost the same as in pure PHCC. The main difference is the clearly in-

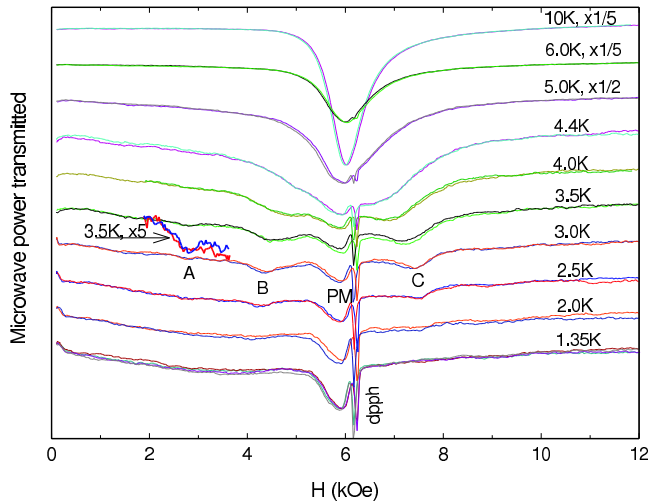


FIG. 4. (color online) ESR absorption spectra for the PHXC with Br concentration  $x = 1\%$ . Spectra are offset for better presentation. Spectral components are marked by the letters in the same way as for the pure compound. High temperature spectra are scaled for better presentation by the factors of  $1/2$  (5.0K) and  $1/5$  (6.0K and 10K), "A" component of the 3.5K spectra is magnified by the factor of 5 for better presentation. Narrow line at 6.2kOe is a DPPH marker ( $g = 2.00$ ), marker position variation on different spectra is due to the frozen fields of the superconducting magnet.  $\mathbf{H}||a^*$ ,  $f = 17.4$  GHz.

creasing linewidth of the spectral components in the doped sample: at 3.0K the half-width at half-height increases for the "A" component from  $0.087 \pm 0.005$  kOe to  $0.106 \pm 0.005$  kOe, for the "B" component from  $0.28 \pm 0.01$  kOe to  $0.37 \pm 0.01$  kOe, for the "C" component from  $0.23 \pm 0.01$  kOe to  $0.37 \pm 0.01$  kOe. As in the case of pure compound, intensity of the "C" component in the 1% doped PHXC slightly exceeds that of the "B" component, which indicates that the effective anisotropy constant is also of the same sign.

### C. ESR on the high-doped PHXC samples $x = 5$ and 10 %.

The temperature evolution of the ESR absorption in the high-doped samples of PHXC with the nominal bromine concentration  $x = 5\%$  and  $10\%$  (Figs.5,6) is qualitatively different from that of the lightly doped sample. At the temperatures above 4 K the intensity of absorption decreases with cooling and the splitting of the ESR line into similar components occurs. But the split components remain clearly visible even at the lowest temperatures. Below we will focus our consideration on the sample with the highest Br concentration,  $x = 10\%$ , the temperature evolution of the absorption spectra for the PHXC sample with  $x = 5\%$  is qualitatively similar to the  $x = 10\%$  case. The half-width of the "A" component for the  $x = 10\%$  PHXC sample is  $0.30 \pm 0.04$  kOe. The

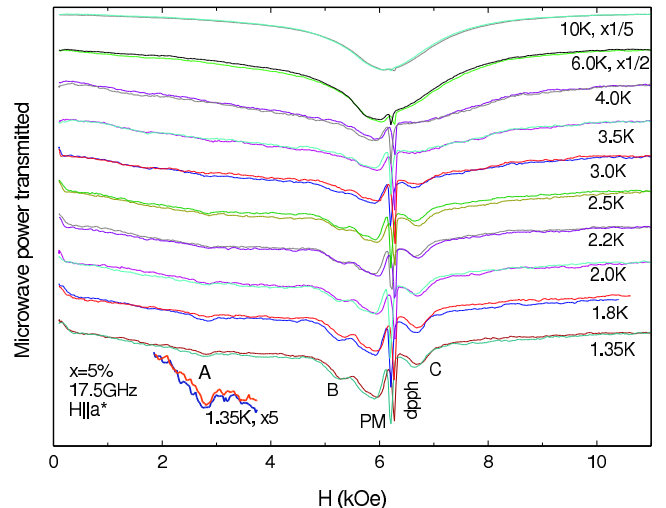


FIG. 5. (color online) ESR absorption spectra for the PHXC with Br concentration  $x = 5\%$ . Spectra are offset for better presentation. Spectral components are marked by letters in the same way as for the pure compound. High temperature spectra are scaled for better presentation by the factors of  $1/2$  (6.0K) and  $1/5$  (10K), "A" component of the 1.35K spectra is amplified by the factor of 5 for better presentation. Narrow line at 6.2kOe is a DPPH marker ( $g = 2.00$ ), marker position variation on different spectra is due to the frozen fields of the superconducting magnet.  $\mathbf{H}||a^*$ ,  $f = 17.5$  GHz.

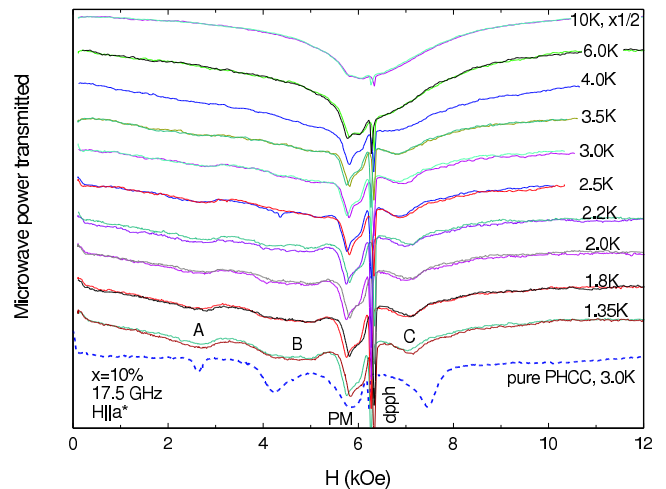


FIG. 6. (color online) ESR absorption spectra for the PHXC with Br concentration  $x = 10\%$ . Spectral components are marked by letters in the same way as for the pure compound. High temperature (10K) spectra are scaled for better presentation by the factor of  $1/2$ . Narrow line at 6.2kOe is a DPPH marker ( $g = 2.00$ ), marker position variation on different spectra is due to the frozen fields of the superconducting magnet. Dashed line shows ESR absorption spectrum of the reference sample with  $x = 0\%$ , amplitudes of the absorption in the reference sample and in the  $x = 10\%$  sample are not in the same scale.  $\mathbf{H}||a^*$ ,  $f = 17.5$  GHz.

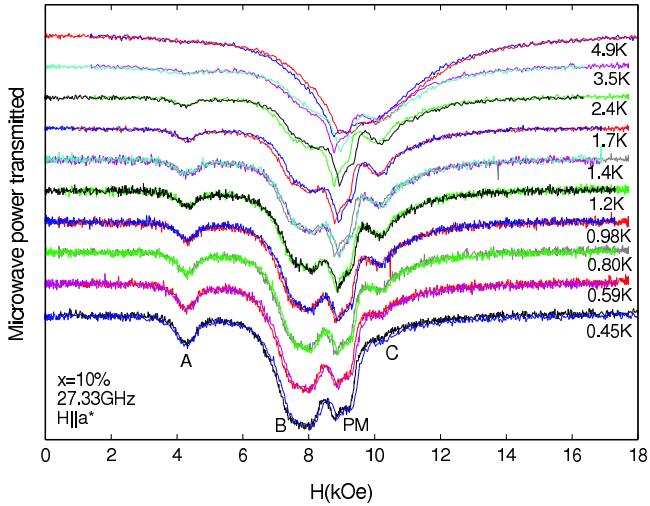


FIG. 7. (color online) ESR absorption spectra for the PHXC with Br concentration  $x = 10\%$  below 1K. The spectra are offset for better presentation. Spectral components are marked by letters in the same way as for the pure compound.  $\mathbf{H} \parallel a^*$ ,  $f = 27.33$  GHz.

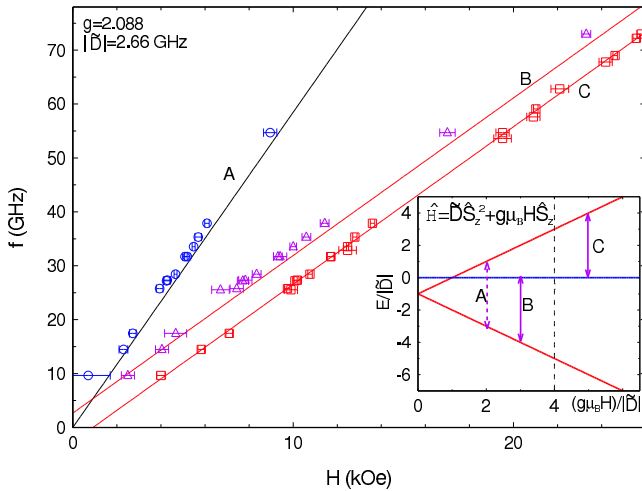


FIG. 8. (color online) Frequency-field dependencies for the PHXC with Br concentration  $x = 10\%$ . Spectral components are marked by letters in the same way as for the pure compound. Solid lines are model curves for the  $S = 1$  in the axial crystal field.  $\mathbf{H} \parallel a^*$ ,  $T = 1.4 \dots 3.0$  K. (Inset) Scheme of the field dependency of the energy levels for the  $S = 1$  center in the axial crystal field for the case of negative anisotropy constant  $\tilde{D}$ . Vertical arrows of the same length mark positions of resonance fields in the experiment with fixed microwave frequency. Different resonance transitions are labelled "A", "B" and "C" in the same way as the absorption components

shape of the absorption corresponding to the "B" component seems to be distorted probably pointing to the superposition of several sub-components, but it can be reasonably approximated by a single lorentzian line with a half-width of 1.0 kOe. The half-width of "C" component is  $0.35 \pm 0.05$  kOe. Splitting of the "B" and "C" compo-

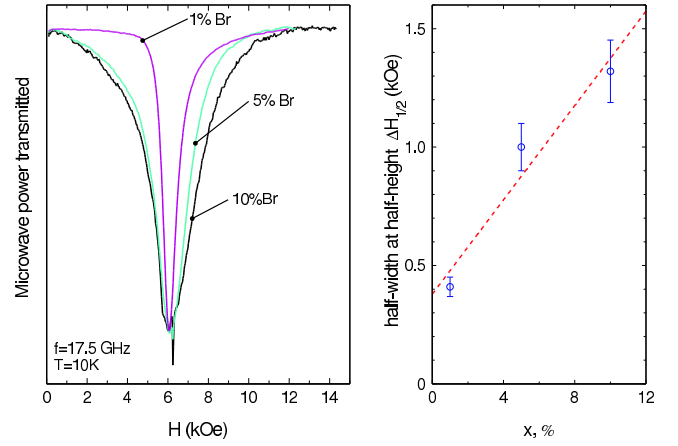


FIG. 9. (color online) ESR absorption spectra at different doping levels (left) and concentration dependency of the half-width at half-height (right). ESR absorption spectra are scaled to the same amplitude for better presentation, narrow absorption line at 6.2kOe is a DPPH marker ( $g = 2.00$ ), dashed line on the right panel is a guide to the eye.  $f = 17.5$  GHz,  $T = 10$  K.

nents is smaller than in the pure compound, it amounts to  $2.4 \pm 0.5$  kOe.

To check whether this absorption signal corresponds to the  $S = 1$  objects or not and to check whether these objects have gapped spectrum or not, we performed measurements at the temperatures down to 450mK on the  $x = 10\%$  doped sample and measured the frequency-field dependency of the observed split ESR absorption signal. These data demonstrate (Fig. 7) that the "A" and "B" components of the split absorption spectrum survive down to the lowest temperatures and gain intensity on cooling, while the "C" component loses intensity below 1K and almost disappears at 450 mK. The frequency-field dependencies for all three modes are in quantitative agreement with the known<sup>23,24</sup> frequency-field dependencies for the  $S = 1$  in the axial crystal field with the effective  $g$ -factor  $g = 2.088$  and effective anisotropy constant  $|\tilde{D}| = 2.7 \pm 0.5$  GHz.

Contrary to the case of the pure and low-doped samples, the integrated intensity of the "B" component at  $T > 1.35$  K slightly exceeds the intensity of the "C" component, this difference became obvious on cooling below 1K (Fig. 7). Thus, the effective anisotropy constant for the high-doped samples has a different sign from that for the pure or low-doped samples.

## IV. DISCUSSION.

### A. Effect of doping on the paramagnetic resonance at $T = 10$ K.

At the temperatures above 5...6K the ESR absorption line for all the samples consists of a single component

and demonstrates an increase of the intensity on heating. This indicates that the ESR absorption at these temperatures is dominated by the triplet excitations of the spin-gap magnet. Comparison of the ESR absorption lines measured at the same temperature  $T = 10\text{K}$  (Figure 9) demonstrates a monotonous increase of the linewidth with doping. As the ESR linewidth is directly related to the lifetime of the spin precession, i.e. to the lifetime of the triplet excitations, this observation is in qualitative agreement with the broadening of the triplet levels and the increase of the magnons damping rate observed in neutron scattering experiments.<sup>19,20</sup>

### B. Estimation of the amount of paramagnetic defects in doped samples.

The ESR spectroscopy allows to separate resonance absorption from the sources with different effective  $g$ -factors. This has an advantage over the "integral" static magnetization measurements where the total magnetization of the sample is measured. This gives us an opportunity to probe the amount of the uncontrolled paramagnetic centers created on doping. These centers are responsible for the "PM" resonance absorption mode.

To estimate the concentration of the paramagnetic centers we scale the integral intensity of the "PM" mode at low temperatures (between 1.5K and approximately 3K) with the total intensity of the ESR at high temperature (10K). The high temperature total intensity can be then scaled to the measured static magnetization (see Eqn.(1)). Then the effective concentration of the paramagnetic centers can be estimated from the Curie law. We have found that the intensity of the "PM" mode in all the samples corresponds to approximately the same amount of about 0.1%  $S = 1/2$   $g = 2.1$  (measured  $g$ -factor) paramagnetic centers per copper ion (Table I). Note that the static magnetization measurements (Figure 1) demonstrate that the low-temperature magnetization of the doped-samples corresponds to the ten-fold higher amount of the paramagnetic defects, i.e. the origin of the low-temperature magnetic response of the doped samples differs from the trivial creation of the additional defects on doping.

The obtained concentration of the paramagnetic  $S = 1/2$   $g = 2.1$  centers is much smaller than the nominal bromine concentration. This independently proves that bromine doping indeed results in the substitution of chlorine ions and not in the creation of additional structural or magnetic defects. This result is in agreement with the X-ray analysis of the doped samples performed in Ref.21.

### C. Nature of the $S = 1$ resonance centers in the high doped samples.

The ESR absorption spectra measured at the lowest temperatures (Fig. 7) prove that the low-temperature

TABLE I. Estimated amounts of paramagnetic centers ( $S = 1/2$ ,  $g \approx 2.1$ ) responsible for the observed intensity of "PM" mode

Nominal Br concentration, %	Amount of paramagnetic centers, % per copper
0	$0.09 \pm 0.01$
1	$0.09 \pm 0.01$
5	$0.06 \pm 0.01$
10	$0.14 \pm 0.03$

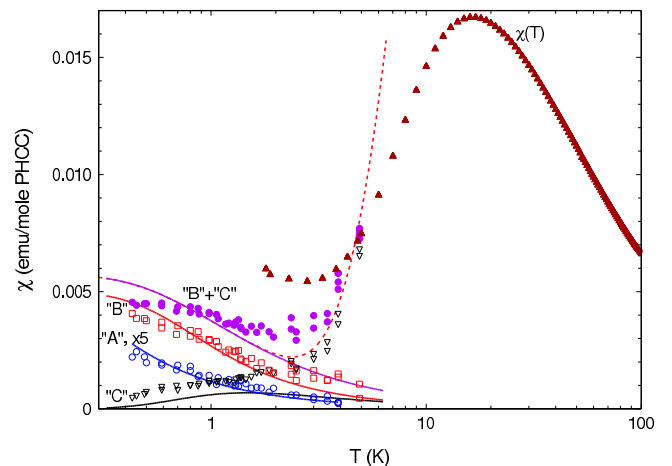


FIG. 10. (color online) Temperature dependencies of the ESR absorption intensities at low temperatures scaled with the high-temperature magnetization for the PHXC sample with Br concentration  $x = 10\%$ . (open circles) Intensity of the "A" component amplified by the factor of 5.0 for better presentation; (open squares) intensity of the "B" component; (open triangles) intensity of the "C" component; (closed circles) total intensity of the "B" and "C" components; (closed triangles) static susceptibility. Curves are fits as described in the text.

absorption in the high-doped samples is dominated not by the gapped triplet excitations or by the paramagnetic  $S = 1/2$   $g \approx 2.0$  defects, but by some other  $S = 1$  objects affected by the effective crystal field  $\hat{H}_{CF} = \tilde{D}\hat{S}_z^2$ . The magnitude of the constant  $\tilde{D} = (-2.7 \pm 0.5)$  GHz and the  $g$ -factor value  $g = 2.088$  are determined from the frequency-field dependency  $f(H)$ , see Figure 8. The negative sign of the  $\tilde{D}$  constant is evidenced by the higher relative intensity of the "B" component as this transition corresponds to the transition from lowest sublevel (see levels scheme on the insert of Figure 8).

If we assume that the  $S = 1$  objects responsible for the low-temperature ESR absorption have no energy gap, then, taking energy of the field independent  $S_z = 0$  sublevel for zero, energies of the  $S_z = \pm 1$  sublevels are  $E_{\pm 1} = \tilde{D} \pm g\mu_B H$ . The temperature dependency of the intensity for each of the resonance absorption components is described by the combination of Boltzmann expo-

nents (Eqn.(2)).

For the "two-quantum" transition "A" this yields

$$I_A \propto \frac{e^{-\frac{\tilde{D}-g\mu_B H}{T}} - e^{-\frac{\tilde{D}+g\mu_B H}{T}}}{1 + e^{-\frac{\tilde{D}-g\mu_B H}{T}} + e^{-\frac{\tilde{D}+g\mu_B H}{T}}} = e^{-\frac{\tilde{D}}{T}} \frac{\sinh \frac{h\nu}{2T}}{2 + e^{-\frac{\tilde{D}}{T}} \cosh \frac{h\nu}{2T}} \quad (3)$$

Note, that the temperature dependency of Eqn.(3) has no fitting parameters: the values of  $\tilde{D}$  and  $g$ -factor are determined in the experiment. The only tunable parameter is the amplitude of the absorption (dependent on the unknown excitation conditions). Experimentally observed intensity of mode "A" is perfectly described by this equation, see Figure 10. This proves that the  $S = 1$  objects, responsible for the low temperature ESR absorption are indeed gapless. It is important to note that since absorption mode "A" is well separated from the position of the  $g = 2.0$  resonance absorption, the determination of the intensity of this mode is not obstructed by the paramagnetic defects.

The main absorption components "B" and "C" correspond to the ordinary  $\Delta S_z = \pm 1$  transitions and are excited by the microwave magnetic field perpendicular to the static field. This allows to analyse quantitatively the intensities of these modes and to estimate the concentration of these gapless  $S = 1$  objects. The scaling factor between the observed absorption intensity and the static susceptibility was calculated at the temperature of 5...6K, which is the highest temperature available in our He-3 experimental setup. At this temperature the intensity of the absorption signal related to the paramagnetic defects is negligible compared to the total intensity. This allows to express the intensities of "B" and "C" components in terms of concentration of the  $S = 1$  objects:

$$I_B = x\Xi \frac{e^{-\frac{\tilde{D}-g\mu_B H}{T}} - 1}{1 + e^{-\frac{\tilde{D}-g\mu_B H}{T}} + e^{-\frac{\tilde{D}+g\mu_B H}{T}}} = x\Xi \frac{e^{\frac{h\nu}{T}} - 1}{1 + e^{\frac{h\nu}{T}} + e^{-\frac{2\tilde{D}}{T}} e^{-\frac{h\nu}{T}}} \quad (4)$$

$$I_C = x\Xi \frac{1 - e^{-\frac{\tilde{D}+g\mu_B H}{T}}}{1 + e^{-\frac{\tilde{D}-g\mu_B H}{T}} + e^{-\frac{\tilde{D}+g\mu_B H}{T}}} = x\Xi \frac{1 - e^{-\frac{h\nu}{T}}}{1 + e^{-\frac{h\nu}{T}} + e^{-\frac{2\tilde{D}}{T}} e^{\frac{h\nu}{T}}} \quad (5)$$

The scaling factor  $\Xi$  ensures the correct Curie dependency of the total intensity at high temperatures ( $T \gg \tilde{D}, g\mu_B H, h\nu$ ):

$$I_{tot} = I_B + I_C \approx \frac{2}{3} x\Xi \frac{h\nu}{T} = x \frac{g^2 \mu_B^2 N_A S(S+1)}{3T} \quad (6)$$

hence  $\Xi = g^2 \mu_B^2 N_A / (h\nu) \approx 1.25 \text{emu}/(\text{mole PHXC})$ .

Experimentally measured intensities of the "B" and "C" modes follow these dependencies reasonably well, best fit is obtained for the concentration of the  $S = 1$  objects  $x = 0.004 \pm 0.001$  per molecule of PHXC. The results of this fit are shown on Figure 10. Determination of the intensities is hindered at low temperatures by the absorption due to the paramagnetic defects. In particular, this leads to the systematic overestimation of the intensity of the weaker component "C". At higher temperatures (above 4K) the observed ESR absorption is dominated by the thermally excited triplets. The temperature dependency of the total ESR absorption intensity in the temperature range 0.45...6K can be fitted by the sum of the contributions from the  $S = 1$  paramagnetic centers and a gapped contribution  $b \times e^{-\Delta/T}$  with the gap value fixed to  $\Delta = 15\text{K}$ , the gap value obtained by the extrapolation of the neutronographic data<sup>19,20</sup> (see dashed line at Figure 10). Note also that, as the temperature increases, the dominating ESR component slowly switches from the low-field "B" component at low temperatures, where the ESR absorption is due to some  $S = 1$  objects, to the higher-field "C" component, as was observed for the triplet excitations in the pure and low-doped samples.

The origin of these  $S = 1$  gapless centers can not be unambiguously recovered from our data. However, the finding that the concentration of these centers is close to 1% per PHXC molecule for the nominal 10% doping suggests following explanation. The building block of the PHCC magnetic subsystem is a  $\text{Cu}_2\text{Cl}_6$  dimer. Two of the chlorine ions are responsible for the intradimer coupling and the four remaining chlorines participate in the formation of the inter-dimer couplings. At the bromine doping level of 10% (assuming uniform doping) the probability to find a dimer with both intra-dimer bond-forming halogens being bromine ions is exactly 1%. A detailed structural analysis of Ref.21 suggested that the occupation of the inter-dimer halogen positions (position  $\text{Cl}_1$  in terms of Ref.21) is slightly less than the nominal value and is about 7.5%, which makes the probability of the double substitution 0.56% even closer to our estimation of the  $S = 1$  objects concentration. Formation of the ferromagnetic bond in the case of the complete supplanting of chlorine ions is in qualitative agreement with the presence of ferromagnetic correlations in the 100% Br-containing crystals.

Finally, we would like to note, that the contribution of the  $S = 1$  spin to the susceptibility exceeds that of the  $S = 1/2$  spin by the factor of 8/3 (spin enters Curie law as  $S(S+1)$ ). Thus, the determined concentration of 0.4% of  $S = 1$  objects per PHCC molecule (or 0.2% per copper ion) corresponds to the concentration of about 0.5% of  $S = 1/2$  centers per copper ion which is reasonably close to the estimation of the low-temperature contribution to the static magnetization. Additional contribution to the static magnetization of the doped PHXC should also arise from the Van-Vleck-like mechanism suggested in Ref.21.

## V. CONCLUSIONS.

We have studied the effect of the bond-doping on the spin-gap magnet  $(\text{C}_4\text{H}_{12}\text{N}_2)(\text{Cu}_2\text{Cl}_6)$  (abbreviated as PHCC). Our experiments show that substitution of the chlorine ions by bromine with doping level up to 10% does not lead to the destruction of the spin gap state. We have shown, that introduction of the bromine ions does not lead to the formation of structural defects — the concentration of the paramagnetic  $S = 1/2$  centers remains practically the same (about or below 0.1%) for the full set of samples from the pure compound to the 10% doped sample.

However, bond-doping affects thermally excited triplet excitations by shortening their lifetime, as evidenced by the increase of the ESR linewidth.

Finally, we have established that the low-temperature ESR absorption is dominated by the  $S = 1$  paramagnetic centers formed with doping. We suggest that these centers are ferromagnetically bound pairs of copper spins appearing when both of the intradimer halogens are substituted by bromine.

## ACKNOWLEDGMENTS

The work was supported by the RFBR projects No.12-02-31220 and No.12-02-00557, Russian Presidential Grant for the Support of the Leading Scientific Schools No.4889.2012.2. This work was partially supported by the Swiss National Fund (division 2).

---

\* glazkov@kapitza.ras.ru

† Current address: National Institute of Chemical Physics and Biophysics, 12618 Tallinn, Estonia

‡ Permanent address: Chemical Department, M.V.Lomonosov Moscow State University, Moscow, Russia

- <sup>1</sup> L.P. Regnault, M. Aïn, B. Hennion, G Dhahlenne, A. Revcolevschi, Phys. Rev. B **53**, 5579 (1996)
- <sup>2</sup> A. Oosawa, M. Ishi, and H. Tanaka, J. Phys. Condens. Matter **11**, 265 (1999).
- <sup>3</sup> Y. Uchiyama, Y. Sasago, I. Tsukada, K. Uchinokura, A. Zheludev, T. Hayashi, N. Miura, and P. Böni, Phys. Rev. Lett. **83**, 632 (1999)
- <sup>4</sup> A. Zheludev, T. Masuda, I. Tsukada, Y. Uchiyama, K. Uchinokura, P. Bni, and S.-H. Lee, Phys. Rev. B **62**, 8921 (2000).
- <sup>5</sup> Ian Affleck Phys. Rev. B **46**, 9002 (1992)
- <sup>6</sup> D. Schmidiger, P. Bouillot, T. Guidi, R. Bewley, C. Kollath, T. Giamarchi, A. Zheludev, Phys. Rev. Lett., **111**, 107202 (2013)
- <sup>7</sup> T. Giamarchi and C. Ruegg, and O. Tchernyshyov, Nature Phys. **4**, 198 (2008).
- <sup>8</sup> O. Nohadani, S. Wessel, S. Haas, Physical Review Letters **95**, 227201 (2005)
- <sup>9</sup> Chandan Dasgupta and Shang-keng Ma Phys. Rev. B **22**, 1305 (1980)
- <sup>10</sup> Daniel S. Fisher Physical Review B **50**, 3799 (1994)
- <sup>11</sup> H. Manaka, A. V. Kolomiets, and T. Goto, Phys. Rev. Lett. **101**, 077204 (2008).
- <sup>12</sup> T. Hong, A. Zheludev, H. Manaka, and L.-P. Regnault, Phys. Rev. B **81**, 060410 (2010).
- <sup>13</sup> E. Wulf, S. Mühlbauer, T. Yankova, and A. Zheludev, Phys. Rev. B **84**, 174414 (2011).
- <sup>14</sup> Rong Yu, Liang Yin, Neil S. Sullivan, J. S. Xia, Chao Huan, Armando Paduan-Filho, Nei F. Oliveira Jr., Stephan Haas, Alexander Steppke, Corneliu F. Miclea, Franziska Weickert, Roman Movshovich, Eun-Deok Mun, Vivien S. Zapf, Tommaso Roscilde arXiv:1109.4403v2
- <sup>15</sup> M.B. Stone, C. Broholm, D.H. Reich, P. Schiffer, O. Tchernyshyov, P. Vorderwisch and N.Harrison, New Journal of Physics **9**, 31 (2007)
- <sup>16</sup> M.B. Stone, I. Zaliznyak, D.H.Reich and C.Broholm Physical Review B **64**, 144405 (2001)
- <sup>17</sup> M.B. Stone, I.A. Zaliznyak, Tao Hong, C.L. Broholm and D.H.Reich, Nature **440**,187 (2006)
- <sup>18</sup> V. N. Glazkov, T. S. Yankova, J. Sichelschmidt, D. Hüvonen, A. Zheludev Physical Review B **85** 054415 (2012)
- <sup>19</sup> D. Hüvonen, S. Zhao, M. Månsson, T. Yankova, E. Ressouche, C. Niedermayer, M. Laver, S. N. Gvasaliya, and A. Zheludev Physical Review B **85**, 100410(R) (2012)
- <sup>20</sup> D. Hüvonen, S. Zhao, G. Ehlers, M. Månsson, S. N. Gvasaliya, A. Zheludev Physical Review B **86**, 214408 (2012)
- <sup>21</sup> D. Hüvonen, G. Ballon and A. Zheludev Physical Review B **88**, 094402 (2013)
- <sup>22</sup> T. Yankova, D. Hüvonen, S. Mühlbauer, D. Schmidiger, E. Wulf, S. Zhao, A. Zheludev, T. Hong, V. O. Garlea, R. Custelcean, G. Ehlers Philosophical Magazine **92**, 2629 (2012) (arXiv:1110.6375v1)
- <sup>23</sup> S. A. Al'tshuler and B. M. Kozyrev, *Electron paramagnetic resonance*, Elsevier Inc., 1964
- <sup>24</sup> A. Abragam, B. Bliney, *Electron paramagnetic resonance of transition ions*, Clarendon Press, Oxford, 1970